Geotechnical Engineering Journal of the SEAGS & AGSSEA Vol. 42 No.3 September 2011 ISSN 0046-5828

Three-Dimensional Deformation Behavior of an Over-Sized Excavation in Shanghai Clay

Y. M. Hou[1, 2], J. H. Wang[1] and D-S Jeng[1, 3, *]
[1] *Center for Marine Geotechnical Engineering, Department of Civil Engineering, Shanghai Jiaotong University, Shanghai 200240, China*
[2] *Shanghai Tunnel Engineering Co. Ltd., Shanghai 200082, China.*
[3] *Division of Civil Engineering, University of Dundee, DD1 4HN, UK*
* *Corresponding author.*
Email address: d.jeng@dundee.ac.uk.

ABSTRACT: In this paper, a case study regarding the excavation of the largest excavation in Shanghai soft clays (Zhongsheng Shopping Mall) is investigated through field studies and numerical modelling. To reduce the excavation induced deformation and construction time, a combination of excavation support schemes, the central part by bottom-up method and the peripheral part by top-down method, is used in this construction project. Extensive field performance data, including wall deflections and ground surface settlements, were collected. Construction sequences are summarized and correlated with the measured data. Three-dimensional effective stress elasto-plastic finite element analysis is conducted to examine the wall deflections and ground surface movements. A comprehensive comparison with the field observations has demonstrated the capacity of numerical models for the predictions of wall deflections and ground surface settlements. Numerical studies indicate that both the wall deflection and ground surface settlement are affected by the excavation corner as well as the length and the shape of the wall. Parametric studies of two construction sequences reveal that the deformations of the wall and soil are larger due to the circumstance that some supports are not installed in time during excavation. Zone excavation exerts a slight effect on the wall deflection for the wall panels near the centers of the excavated zones, but causes less wall deflection for the wall panels near the corners of the excavated zones.

Keywords: Over-sized excavation, combined method, deformation, three-dimensional, finite element analysis

1. INTRODUCTION

Recently, to meet the increasing demand for economic growth, extensive underground structures have been rapidly constructed in Shanghai. For those large excavations in sensitive areas, complex construction sequences are generally adopted to limit the excavation induced deformations and to protect the adjacent structures and utilities. The excavation for Zhongsheng Shopping Mall currently is the largest excavation in Shanghai district. The dimension of the excavation was 250 m (length)x 235 m (width)x13.8 m (depth). The total area of the excavation was about 50000 m^2. To control lateral displacements of the earth retaining structures and reduce construction time, this excavation was constructed by using a combination of two schemes ‧the bottom-up method in the central part and the top-down method in the peripheral part.

Deep excavation in soft clays normally causes large deformations of the surrounding soil that could further damage the adjacent properties. To understand the excavation deformation characteristics, numerous researchers investigated the wall deflections, surface and subsurface soil movements, pore pressures, and struts load through field observation of case histories (Finno et al., 2002; Finno and Roboski, 2005; Liu et al., 2005; Ou et al., 1998). Finite element analysis has been employed to study the characteristics of wall deformations, predictions of ground movement, and three-dimensional (3-D) effects of the excavation, the detailed structural system and complex construction sequences (Finno and Harahap, 1991; Finno et al., 2007; Whittle et al., 1993; Hashash and Whittle, 1996; Ng et al., 1998; Ou et al., 2000). Most previous investigations concerned the typical-sized excavation constructed using either the bottom-up excavation method or the top-down excavation method. To the authors' best knowledge, research considering combination of two excavation support schemes hasn't been available in the literature yet.

In this study, both the field observations and numerical simulation for an over-sized excavation involving a combination of both top-down and bottom-up support systems will be presented. The details of the support system of the excavation, subsurface conditions at the site, and the construction sequence will be described first. Extensive field monitoring/performance data, including wall deflections and ground surface settlements, are collected. Then, a three-dimensional finite element model for the entire excavation site, mimicking detailed construction sequences, will be developed and calibrated by the observed wall deflections and ground surface settlements data. Furthermore, a set of FEM parametric study for the effects of the construction sequence and zone excavation on the excavation deformation will be carried out. Based on both field observation data and FEM analysis results, several key findings will be concluded.

2. Field Study

2.1 Site conditions

The Zhongsheng Shopping Mall is located in the southwest of Shanghai and occupies an area of about 50000 m^2. The building has five above-ground stories devoted to shopping mall uses and three underground levels for parking. Figure 1 shows the layout of the construction site as well as the different construction zones as indicated by the central part and the eleven zones in the peripheral part of the excavation. The excavation site is approximately trapezoid in shape with maximum excavation depth as 13.8 m. A 0.8 m thick and 23.5 m deep concrete diaphragm wall was used as the earth-retaining structure. The central part occupied an area of about 21,000 m^2 and was constructed with the bottom-up method, while the peripheral part occupied an area of about 29,000 m^2 and constructed with the top-down method.

The construction site was underlain by thick, relatively soft, quaternary alluvial and marine deposits. Figure 2 summarizes the stratigraphy at the site. The first and second layers were fills, consisting mainly of a medium dense sand layer and a 1.8 m thick clay layer. A sandy silt layer was underneath the clay layer. Beneath the sandy silt layer, there were five layers of silty clay with a total thickness of 23.6 m, which exert predominant effects on the observed excavation behavior in the Zhongsheng Shopping Mall case history. The subsequent soil layers were a sandy silt layer and a fine sand layer.

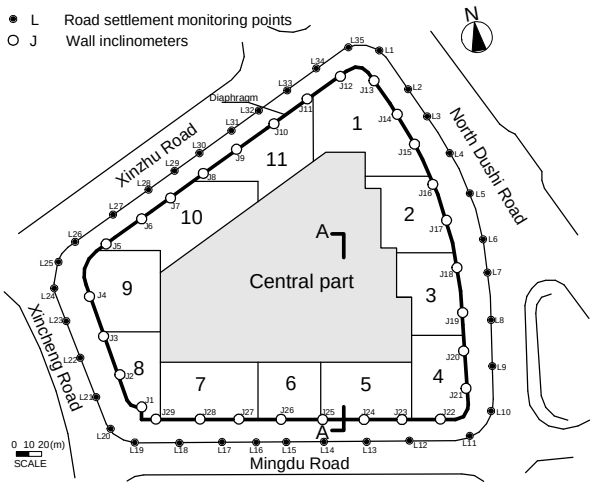

Figure 1 The location and instrumentation of the excavation site

The groundwater table was at about 1 m below ground level. In Figure 2, the variation of soil properties, i.e., the soil unit weight, the water content, the void ratio of the soils, the compression index of the soils, the un-drained shear strength, and the pre-consolidation pressure, with the depth are illustrated. The shear strength of the clay soil was obtained from in-situ vane shear tests. It can be seen that most of the soils in this excavation site are clays with high water content and low shear strength.

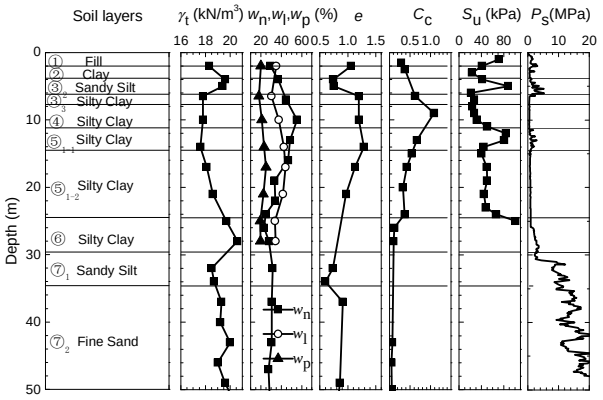

Figure 2 Soil profiles and variation of geotechnical parameters with depth.

2.2 Construction sequence

The excavation was completed in seven stages. Figure 3 illustrates the cross section A-A at stages 2, 3, 5, and 7 (final stage), respectively. The bottom-up method was used for the central part of the excavation, while the top-down method was adopted to excavate the peripheral part. Three levels of concrete floor slabs were employed to support the diaphragm walls at depths of 0.00 m, -5.65 m and -9.35 m. The time sequence of construction activities for this project is summarized in Table 1.

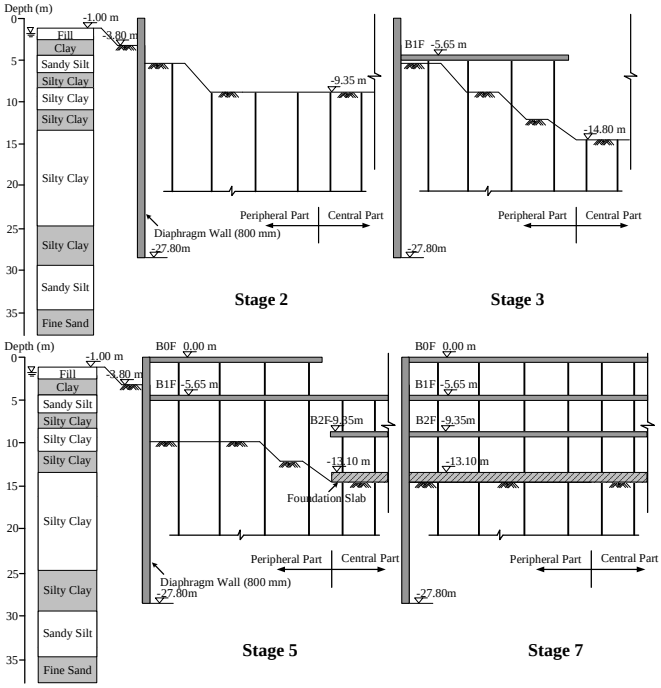

Figure 3 Cross section A-A during several excavation stages

Table 1 Construction sequence of the excavation.

Stage	Interval (days)	Construction operation
1	235	Excavate to elevation of -3.80 m and construct diaphragm wall and pile foundation
2	118	Excavate the central part to -9.35 m and excavate the peripheral part (zone 1~11) to -6.60 m
3	136	Cast the floor slab (B1F) of zone 1, 2, 4, 5, 7, 8, and 9 at elevation of -5.65 m, zone 10 and 11 were braced by concrete struts, excavate the central part to -14.8 m
4	106	Complete the floor slab (B1F) of zone 3 and 6, cast floor slab (B0F) of zone 1, 2, 3, 5, 6, 7, 9, and 11 at elevation of 0.00 m, cast the foundation slab and the floor slab (B2F) at elevation of -9.35 m of the central part
5	111	Cast the floor slab (B1F) at elevation of -5.65 m of the central part, excavate the peripheral part (zone 1~11) to -10.35 m
6	37	Cast the floor slab (B2F) at elevation of -9.35 m of the peripheral part (zone 1~11) and complete the floor slab (B0F) at elevation of 0.00 m of zone 4, 8, 10 and central part
7	109	Excavate the peripheral part (zone 1~11) to -14.80 m and cast the foundation slab of the peripheral part

As revealed in Table 1, the central part of the pit was excavated to the bottom (-14.8 m) after the concrete floor slab (B1F) at elevation of -5.65 m of the peripheral part was cast at stage 3. Thereafter, three levels of concrete floor slabs and the foundation slab of the site's central part were cast using the bottom-up method while the peripheral part was constructed using the top-bottom method. Prior to the peripheral part of the site was excavated to the

bottom at stage 7, three levels of concrete floor slabs had been cast completely.

To reduce the wall deflections during the construction, the peripheral part of the excavation was carried out by zones (see Figure 1) at stage 2 before the concrete floor slab (B1F) of the peripheral part located at elevation of -5.65 m was cast. During the zoned excavation, the zones near the corner of the diaphragm wall (zones 1, 2, 4, 5, 7, 9, 10) were first excavated. On reaching the prescribed level in these zones, the concrete floor slabs (B1F) were then cast. Thereafter, the zones near the center of the excavation (zones 3, 6, 8, 11) were excavated, and supported with the concrete floor slab (B1F). It is noted that the concrete floor slabs of some zones were not installed in time after soil was excavated and the excavation in zones 10 and 11 were supported with concrete struts.

2.3 Field observation

To study the performance of the excavation, various instruments were installed on site, as shown in Figure. 1. Twenty-nine inclinometer tubes whose length was equal to the depth of the diaphragm wall were affixed to the steel reinforcement cages and concreted at various critical locations of the wall. The rotation of the diaphragm wall was measured at 1 m intervals along its depth to observe the wall deflection. Therein, inclinometers J1~J4 were installed in the west wall, J5~J12 were installed in the north wall, J13~J21 were installed in the east wall, and J22~J29 were installed in the south wall of the excavation. To determine absolute displacements of the diaphragm wall, the movements at the top of the wall were surveyed by a theodolite and a horizontal reference line. To monitor the influence of the excavation activities on the surrounding environment, thirty-five surface survey points were installed along four surrounding roads prior to the main excavation. The distance between the survey points and the diaphragm wall varied from 12 m to 26m.

Deformation of diaphragm wall

The absolute displacement profiles of the wall during the main excavation were deduced from the measured movement at the top of the wall that had been monitored throughout the construction period by using a theodolite and precise taping. Figure 4 shows typical lateral wall deflections at representative inclinometers J3, J9, J17 and J26 which were respectively installed in the mid-span of the four walls prior to the main excavation. At stage 2 of the main excavation, the diaphragm wall was not propped and behaved effectively as a cantilever, in which the maximum lateral displacement occurred at the top level of the wall. At stage 5 the floor slab (B1F) was completed. The diaphragm wall at J3, J9, J17, and J26 rotated with respect to the position of the floor slab (B1F) because the high axial stiffness of the slab prevented the wall from moving at that position. As the excavation proceeded, deep inward displacement gradually developed at all walls, with the maximum wall displacement occurring near the excavation surface.

After the final excavation depth was reached, deep-seated deflected shapes of the walls were observed, and the maximum wall displacements occurred within a few meters above the final excavation level at all walls. The ratios between the maximum lateral displacement and the excavated depth were in the range of 0.0053-0.0075. As indicated in Fig. 4, the lateral displacement observed at the north wall (J9) is greater than those at the other walls, which could be attributed to the maximum length of the north wall and the relatively small stiffness of the concrete strut (B1F) at zone 10 and 11.

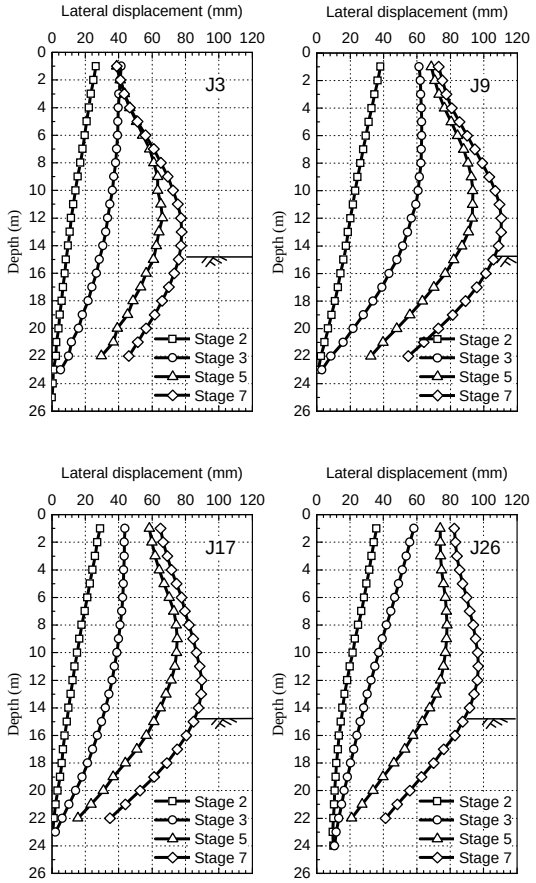

Figure 4 Variation of wall lateral displacement at inclinometers J3, J9, J17 and J26.

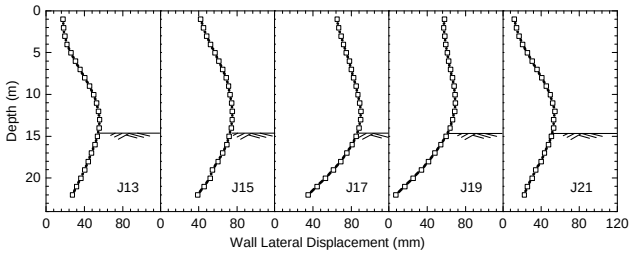

Figure 5 Lateral displacement of the east wall at final stage.

Fig. 5 summarizes the measured lateral displacement of the east wall along the North Dushi Road at final stage. The 3-D behavior of the diaphragm wall is illustrated clearly in this figure. The maximum wall deflections at J13 and J21 near the corners were 55.7 mm and 54.6 mm, respectively. The maximum wall deflections at J15 and J19 were similar, which were 74.9 mm and 75.3 mm, respectively. The maximum wall deflection at J17 near the mid-span of the wall was 89.7 mm. There is a significant reduction in lateral displacement as one moving from the mid-span towards the corner of the excavation, which is similar to the 3-D behavior of the diaphragm wall reported by Ou et al. (1998) and Finno et al. (2007). As shown in Figure 5, the lateral displacement at the top level of the wall at J19 is much larger than that at J15, while the maximum lateral displacements at these two inclinometers are similar, which is different from the references reported by Ou et al. (1998) and Finno et al. (2007). This is perhaps attributed to the fact that the floor slab (B1F) at Zone 3 affecting J19 was not cast in time.

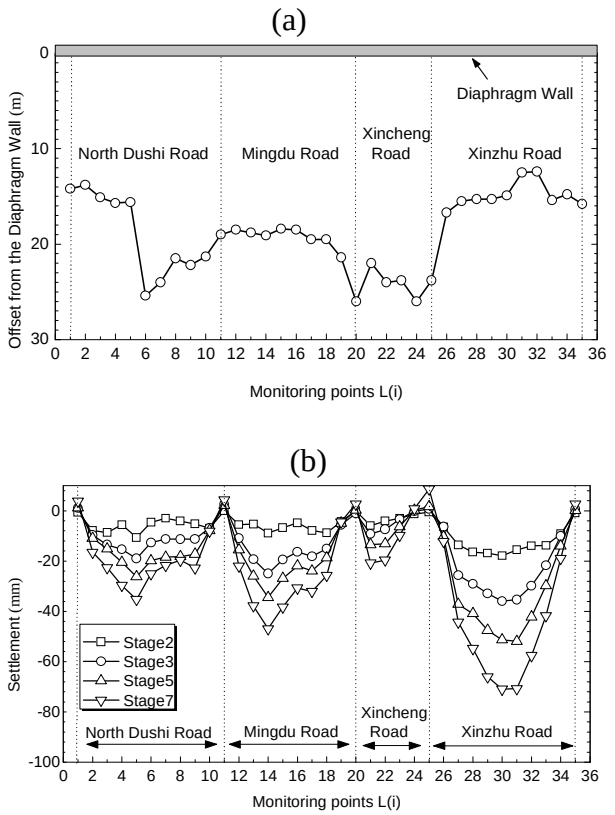

Figure 6 Ground surface settlement along the roads around the excavation.

Ground surface settlement

Figure 6 shows the ground surface settlement distribution along the roads surrounding the excavation site at various stages. The data represents optical survey points located 12 m~26 m from the diaphragm wall, as shown in Figure 6(a). The general settlement patterns were very similar along four sides of the site, with apparent U-shaped settlement profile. 3-D effect of the ground surface settlement became more apparent as the excavation depth was increased, suggesting that the stiffening effects of the corners became more pronounced as the excavation proceeded. The settlements near the corners were much smaller than those near the center, and this observation was consistent with that noted by Lee et al. (1998). The maximum settlement along North Dushi Road was 35 mm, compared to 47 mm along Mingdu Road, 21 mm along Xincheng Road, and 71 mm along Xinzhu Road. It could be observed that the ground surface settlement at L4 behind the North Dushi Road is obviously smaller than the settlement at L28 behind the Xinzhu Road although two points is installed at the similar location from the diaphragm wall. This is perhaps attributed to the fact that the floor slab (B0F) at Zone 10 affecting L28 was not cast in time.

3. Numerical Study

3.1 Three-dimensional (3-D) finite element analysis

It has been well reported in the literature that plane strain analysis normally yields conservative results, while a 3-D analysis can realistically simulate the actual excavation behavior (Ou et al., 1996; Zdravkovic et al., 2005). It has been reported that a précised prediction of the ground settlement, which often requires proper modeli ng of clay behavior, is more difficult than wall deflection, and that accurate prediction of ground settlement. Numerical simulation considering the small-strain non-linearity of soil with high initial stiffness and stiffness degradation inside the initial yield surface could improve the predicting accuracy of the excavation deformation.

In this study, our primary objective was primarily to exam the effects of construction sequence, the zoned excavation in a large over-sized excavation, the combined support scheme involving both top-down and bottom-up supporting systems, and 3-D effects through a numerical modeling. . The 3-D finite element analysis was therefore carried out using the program ABAQUS to investigate the deformation behavior of the excavation for the case study of the Zhongsheng Shopping Mall.,

Figure 7 shows the 3-D finite element mesh used for the analysis. The excavation site of the Zhongsheng Shopping Mall case was modeled as a block measuring 1,250×1,250 m in plan area and 80 m deep. Such a large zone was selected to avoid any measurable effects from the boundaries in the final results. In this case study, the model included the soil, diaphragm wall, floor slabs, concrete struts, and piles. The soils were modeled using 3-D hexahedral elements. The diaphragm wall and concrete floor slabs were modeled using structural shell elements. The concrete struts and piles were simulated by structural beam elements. Beam elements were 1-D line elements in 3-D space that offered stiffness associated with axial stretch, curvature change, torsion, and transverse shear deformation. The cross-sections of the beam elements were adopted according to the geometry of the concrete struts and piles. During the simulation, the adopted cross sections of concrete struts and piles could not deformation in their own planes. To reduce the computational time, linear-order elements (8-noded element) were used in the numerical modelling. The entire model includes 146,480 elements and 162,615 nodes. The vertical boundaries of the model were supported with rollers, while the bottom boundary was constrained with hinges.

(a) Finite element mesh of the model

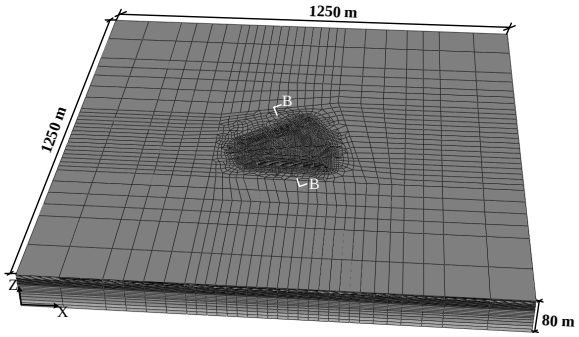

(b) Cross-section B-B of the model at stage3

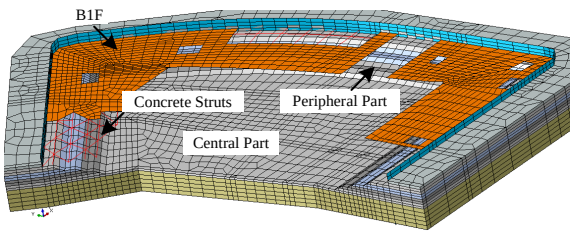

Figure 7 Numerical model of the excavation.

In the analysis, the simple Mohr-Coulomb elasto-plastic model was used to simulate the sand layers while the modified Cam-Clay model, as proposed by Roscoe and Burland (1968), was used for clay layers. The use of a simpler MCC model in this numerical simulation is based on the following reasons. First, the large mesh size used to model the 3-D excavation has led to the use of linear order element. Second, there are many more parameters used in the model to be characterized for small strain nonlinearity model; which are not available from standard laboratory tests for this construction

project. In addition, the components of the consistent Jacobian cannot be expressed analytically by exact linearization of the constitutive equations for the small strain nonlinearity model. To overcome this difficulty, explicit integration generally is adopted, which would result in a significant amount of analysis sub-steps and computational cost.

Table 2 Soil parameters used in numerical analysis.

(a) Modified Cam-Clay model

Layer No.	Unit weight γ (kN/m^3)	Swelling index κ	Compression index λ	ϕ (^{o})	v	Interface frictional resistance τ_{max} (kPa)
①	19.10	0.010	0.12	32	0.30	20
②	18.85	0.010	0.12	32	0.30	20
③	17.85	0.008	0.10	29	0.35	20
③	17.85	0.028	0.32	29	0.35	20
④	17.15	0.033	0.40	18	0.40	22
⑤	18.25	0.023	0.27	32	0.35	35
⑤	18.25	0.018	0.22	32	0.35	35
⑥	19.80	0.010	0.13	30	0.30	62

(b) Mohr-Coulomb model

Layer No.	Unit weight γ (kN/m^3)	Yong's modulus E (MPa)	c (kN/m^2)	ϕ (^{o})	v	--
$⑦_1$	19.25	70	6.70	33	0.30	--
$⑦_2$	19.25	95	6.70	33	0.30	--

The soil parameters used in the analysis are tabulated in Table 2. With the MCC model, the shear modulus is defined from the bulk modulus and Poisson's ratio as

$$G = \frac{3(1-2\nu)(1+e_0)}{2(1+\nu)\kappa}(p + p_t^{el})\exp(\varepsilon_{vol}^{el}) \quad (1)$$

where e_0 is the initial void ratio, p is the equivalent pressure stress, p_t^{el} is the elastic tensile strength, ε_{vol}^{el} is the logarithmic measure of the elastic volume change.

With the Mohr-Coulomb elastic-plastic model, the Yong's modulus was computed using the empirical formula (Japanese Geotechnical Society, 1992)

$$E = 25 P_a N \quad (2)$$

where P_a is the atmospheric pressure, and N is the standard penetration resistance (SPT) number.

Soil properties in Table 2 were based on the site investigation. The compression indexes were calculated firstly by Cc in Fig. 2. Based on the calculated values, back - analysis was executed to determine the compression index and the swelling index by matching the calculated and measured wall deflections, as shown in Table 2. According to the parameters analysis, it could be found that the compression index λ was insensitive to the wall deflection. The wall deflection was mainly influenced by the swelling index κ, and the ground surface settlement was influenced by both parameters. The retaining diaphragm wall, concrete struts, and concrete floor slabs were assumed to behave as linear-elastic materials. Considering that concrete may crack as a result of deformation, stiffness of the structures was reduced by multiplying the nominal stiffness by a reduction factor. Ou and Shiau (1998) reported that the value of the reduction factor could be reasonably assumed to be 0.6. Thus, the Young's modulus of the structures used in the analysis was 18,000 MPa and the Poisson's ratio was assumed to be 0.2.

To consider the slip between the diaphragm wall and the soil, interfaces were created between the diaphragm wall and surrounding soils. The ultimate frictional resistances of the interfaces were adopted according to the ultimate frictional resistances of the bored piles suggested by Code for Investigation of Geotechnical Engineering in Shanghai (DGJ08-37-2002), as listed in Table 2. The friction coefficients were empirically assigned as 0.2 for all interfaces. Based on a separate sensitivity analysis, it was found that the wall deflections and ground settlements were not sensitive to the interface friction coefficients.

The FE analysis was performed in a step-by-step procedure following the actual excavation sequence given in Table 1. The excavations at stage 1, 2, 3, 5, and 7 were simulated by removal of soil elements. At each time of such excavation, the excavated surface was made stress free by calculating the equivalent nodal forces from the removed elements and applying them on the excavated boundary (Ishihara, 1970). Although the lateral supports elements could not be created within an analysis directly, a similar effect could be achieved by creating them in the model definition, removing them at the first step, and subsequently reactivating corresponding structural elements at stage 3~7. It is noticed that some lateral supports were not installed in time. The shell elements of floor slabs (B1F) in zone 3 and 6 were reactivated at stage 4 while the other shell elements of floor slabs (B1F) were re-activated at stage 3. The shell elements of floor slabs (B0F) in zone 4 and 10 were reactivated at stage 6 while the other shell elements of floor slabs (B0F) were reactivated at stage 4.

3.2 Numerical results

A comparison of wall deflections between numerical analysis and the field measurements at inclinometers J3, J9, J17, and J26 at final stage of the main excavation is illustrated in Figure 8. It can be seen that the numerical predictions of the wall deflections overall agree with the measurements.

However, the finite element model over-predicts the lateral inward movement in the region of the toe at J17 and J26. The lateral inward movements at the top level of the wall are also over-predicted at J9 and J26, which resulted in smaller computed wall curvature than the measured value. The maximum difference between the measured and calculated results is about 18% at J9.

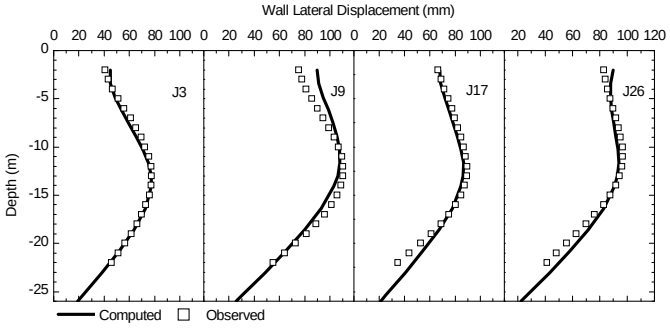

Figure 8 Comparison of the observed and computed wall deflections at final stage.

Table 3 Summary of relative differences between the measured and predicted ground settlements at different construction stages.

Stage	Monitoring Points (%)					
	L1	L2	L3	L4	L5	L6
Stage 3	291	1.2	0.4	9.9	6.7	22.1
Stage 5	340	33.8	33.5	22.7	14.9	16.4
Stage 7	199	12.1	27.3	7.3	8.2	16.7
	L13	L14	L15	L16	L17	L18
Stage 3	9.3	6.4	18.5	20.4	12.5	7.5
Stage 5	21.2	14.9	27.1	34.2	27.5	29.6

Stage 7	5.2	6.8	12.8	21.0	19.9	18.9
	L25	L26	L27	L28	L29	L30
Stage 3	545	22.3	25.9	3.2	23.5	22.4
Stage 5	392	13.1	5.6	9.4	7.6	2.1
Stage 7	169	20.3	11.3	3.3	8.2	18.6

Stage	Monitoring Points (%)					
	L7	L8	L9	L10	L11	L12
Stage 3	31.0	19.5	10.8	125	167	22.8
Stage 5	19.4	10.7	7.8	127	218	29.2
Stage 7	29.5	29.5	3.3	172	178	29.5
	L19	L20	L21	L22	L23	L24
Stage 3	21.3	135	27.3	30.4	32.1	271
Stage 5	34.5	1589	30.3	9.8	26.7	469
Stage 7	87.8	279	10.5	14.8	13.6	275
	L31	L32	L33	L34	L35	
Stage 3	0.6	11.0	14.3	23.1	369	
Stage 5	1.0	6.2	6.7	32.3	2105	
Stage 7	0.6	13.0	16.2	23.3	221	

The relative differences between the measured and predicted ground settlements at different construction stages are summarized in Table 3. It could be found that the means of bias between the measured and predicted data are 16.1%, 18.3%, and 14.9% for all measured points except corner points at stage 3, 5, and 7, respectively. The standard deviations of bias are 53.2%, 52.5%, and 45.8% at stage 3, 5, and 7. All corner points are way off which could be attributed to two reasons. First, the measured settlements at the corner points are relatively small, which induces the percentage of difference magnified. Second, there were measured swelling at the corner which could not be reflected from the numerical results.

Based on the findings presented by Clough and O'Rourke (1990), the concave-type settlement profile was generally observed for braced excavations in soft to medium clays. Figure 9 illustrates a comparison of the ground settlement at final stage of excavation between observations, Clough and O'Rourke model and the present model, in which the observed (inverse triangle), the present model (solid line), and the trends established by Clough and O'Rourke (dashed line) for.

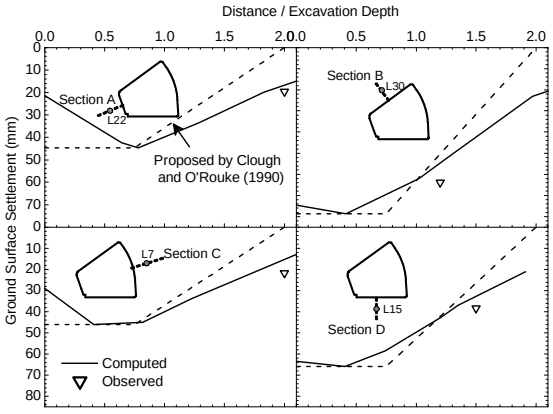

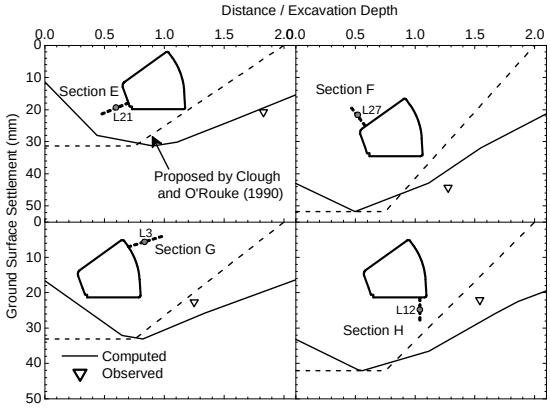

Figure 9 Observed and computed ground surface settlements at final stage.

It could be found that the prediction of ground settlement from the present model is close to the observed settlement. The method of Clough and O'Rourke (1990) generally gives a good estimate of the settlement envelope within a distance not greater than 1.0 times of the excavation depth. When the distance exceeds 1.0 times of the excavation depth, the Clough and O'Rourke method generally underestimates the ground surface settlement.

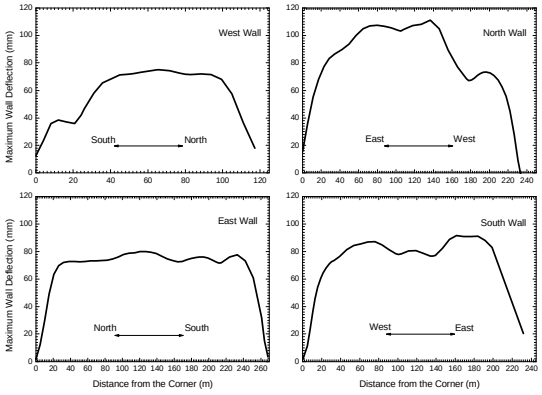

Figure 10 Calculated maximum wall deflections at final stage.

Figure 10 shows the variation of calculated maximum wall deflection with the distance from the corner for the final stage of the excavation. The 3-D deformation behavior of the diaphragm wall is illustrated clearly in this figure. It can be seen from the figure that deformation behavior of the diaphragm wall is affected by the corners. The wall deflections near the corners are much smaller than those near the centers. The distance from the corner to a section having plane strain behavior is similar for four sides of the diaphragm wall, and the distance ranges from 30m to 50m. It could be noticed that there are some irregular bumps on the wall deflection curves which could be attributed to the access openings at the supporting slabs and some lateral supports not installed in time. The maximum deflections of the east, north, west, and south wall are 75.0 mm, 107.3 mm, 80.1 mm, and 87.1 mm, respectively. The maximum deflection of the west wall is relatively small compared with the other walls due to the minimum length of the wall. The maximum wall deflection of the north wall is 23.2% larger than the south wall although their lengths are similar. This can be attributed to the lateral supports of zone 10 and 11 with less stiffness and the lateral supports of zone 10 not installed in time. For the east wall with an arch shape, the wall deflection is a little larger than the south wall. It could be concluded that the arc shape has insignificant effect for limiting the deflection of the diaphragm wall when the radius of curvature is too large.

3.3 Effect of construction sequences

As shown in Table 1, some concrete floor slabs were not cast in time during the process of the main excavation, which could cause more wall deflection and ground surface settlement. To investigate the effects of these concrete floor slabs on the performance of the excavation, another type of 3-D finite element analysis, assuming that all supports were installed in time, was performed. Figure 11 compares the calculated wall lateral displacement at J3, J9, J17, and J26 for both the actual and assumed construction sequences when the excavation reaches final depth. The maximum calculated wall lateral displacement for the assumed excavation sequence also occurred at J9 and is approximately 96 mm when the excavation is completed. The maximum wall deflections of the assumed case are 9.5%, 10.4%, 9.2%, and 9.3% smaller than those of the actual case at J3, J9, J17, and J26, respectively. The ratios between the maximum lateral displacement and the excavated depth for the assumed construction sequence are in the range of 0.0047-0.0065.

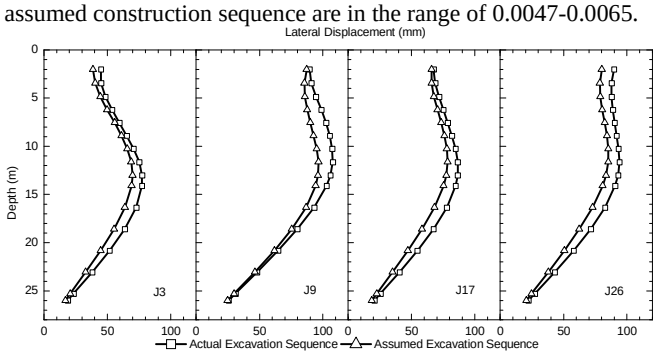

Figure 11 Comparison of computed wall deflections for two construction sequences.

Zoned excavation may result in less wall deflection and ground surface settlement due to the corner effect of the excavation. For the Zhongsheng Shopping Mall case history, zoned excavation was employed for the peripheral part of the excavation before the concrete floor slab (B1F) of the peripheral part was cast. To study the effect of zoned excavation on the excavation deformation behavior, two types of 3-D finite element analysis, zoned excavation and un-zoned excavation, were performed. The un-zoned excavation sequence is a uniformly staged excavation, with the entire peripheral part of the site excavated to the prescribed levels and then all the concrete floor slabs (B1F) of the peripheral part installed.

Figure 12 presents the comparison of the calculated wall deflections and the ground surface settlement for both the zoned and unzoned excavation sequences. As indicated in this figure, the maximum wall deflections at J3 and J26 are 70 mm and 85 mm for unzoned excavation case, which are 14% and 4.7% smaller than those of the zoned case, respectively.

It could be found that zoned excavation only slightly affect the wall deflections for the wall panels near the centers of the excavated zones, such as J26. However, zoned excavation causes less wall deflections for the wall panels near the corners of the excavated zones, such as J3. This can be explained that the wall lengths along the excavated zones are so large that the wall deflections near the zone centers would not be affected by the corners. Wall deflections near the centers of the excavated zones due to zoned excavation are thus relatively close to those of the case of the un-zoned excavation. For the wall panels near the corners of the excavated zones, wall deflections are affected by the corners in zoned excavation while the corresponding wall deflections are relatively close to those of the plain strain condition in un-zoned excavation. Wall deflections using zoned excavation are thus less than those using un-zoned excavation. The ground surface settlements also exhibit a similar behavior.

4. Conclusions

In this paper, a case history of an over-sized excavation in Shanghai soft clays is presented. The excavation was constructed using a combination of two methods: bottom-up method for the central part and top-down method for the peripheral part. Based on the in-situ observation and 3-D nonlinear finite element analysis, the following conclusions can be drawn:

1. For the over-sized excavation supported by the combination of top-down and bottom up excavation support mechanisms, the diaphragm wall behaved as a cantilever before the concrete floor slab (B1F) was cast completely. Thereafter, deep inward movements developed for the wall as the excavation proceeded. The maximum wall displacements occurred near the final excavation level. The ratios between the maximum lateral displacement and the excavated depth were in the range of 0.0053-0.0075.
2. Based on the field observations and the finite element analysis, the wall deformation behavior is affected by the corners, the construction sequence, the length, and shape of the diaphragm walls. The distance from the corner to a section having plane strain behavior ranges from 30m to 50m for diaphragm walls.
3. The ground surface settlements of the excavation supported by the combination of top-down and bottom up excavation support mechanisms could be reasonably predicted. The method of Clough and O'Rourke envelopes the settlement profile within the distance of 1.0 times the excavation depth. When the distance exceeds 1.0 times of the excavation depth, the method generally underestimates the ground surface settlement.
4. Based on the finite element analysis, zoned excavation at the first excavation stage exerts a slight effect on the wall deflections for the wall panels near the centers of the excavated zones. however, it causes less wall deflections for the wall panels near the corners of the excavated zones while the wall length along the excavated zones is too large. The circumstance that some lateral supports not installed in time may result in larger deformation of the over-sized excavation supported by the combination of top-down and bottom up excavation support mechanisms.

Acknowledgments

The authors are grateful for the financial support from the National Science Foundation of China (No. 50679041) and Shanghai Leading Academic Discipline Project (No. B208).

4. REFERENCES

Clough, G. W. and O'Rourke, T. D. (1990) Construction-induced movements of in situ walls. Proceedings, Design and Performance of Earth Retaining Structures, Ithaca, N. Y. American Society of Civil Engineers, Special Publication, pp. 439-470.

Finno, R. J. and Harahap, I. S. (1991) Finite element analysis of HDR-4 excavation. Journal of Geotechnical Engineering, ASCE, Vol. 117, No. 10, pp. 1590-1609.

Finno, R. J., Bryson, S. and Calvello, M. (2002) Performance of a stiff support system in soft clay. Journal of Geotechnical and Geoenvironmental Engineering, ASCE, Vol. 128, No. 8, pp. 660-671.

Finno, R. J. and Roboski, J. F. (2005) Three-dimensional responses of a tied-back excavation through clay. Journal of Geotechnical and Geoenvironmental Engineering, ASCE, Vol. 131, No. 3, pp. 273-282

Finno, R. J., Blackburn, J. T. and Roboski, J. F., (2007) Three-dimensional effects for supported excavations in clay. Journal of Geotechnical and Geoenvironmental Engineering, ASCE, Vol. 133, No. 1, pp. 30-36.

Hashash, Y. M. A. and Whittle, A. J., (1996) Ground movement prediction for deep excavations in soft clay. Journal of Geotechnical Engineering, ASCE, Vol. 122, No. 6, pp. 474-486.

Ishihara, K. (1970) Relations between process of cutting and uniqueness of solution. Soil and Foundations, Vol. 10, No. 3, pp. 50-65.

Japanese Geotechnical Society. (1992) N value and c and φ, considerations and applications. Japanese Geotechnical Society Press.

Lee, F. H., Yong, K. Y., Quan, C. N. and Chee, K. T. (1998) Effect of corners in strutted excavations: Field monitoring and case histories. Journal of Geotechnical and Geoenvironmental Engineering, ASCE, Vol. 124, No. 4, pp. 339-349.

Liu, G. B., Ng, C. W. W. and Wang, Z. W., (2005) Observed performance of a deep multistrutted excavation in Shanghai soft clays. Journal of Geotechnical and Geoenvironmental Engineering, ASCE Vol. 131, No. 8, pp. 1004-1013.

Ng, C. W. W., Simpson, B., Lings, M. L. and Nash, D. F. T. (1998) Numerical analysis of a multipropped excavation in stiff clay. Canadian Geotechnical Journal, Vol. 35, pp. 115-130.

Ou, C. Y., Chiou, D. C. and Wu, T. S., (1996) Three-dimensional finite element analysis of deep excavations. Journal of Geotechnical Engineering, ASCE; Vol. 122, No. 5, pp. 337-345.

Ou, C. Y. and Shiau, B. Y. (1998) Analysis of the corner effect on the excavation behavior. Canadian Geotechnical Journal, Vol. 35, No. 3, pp. 532-540.

Ou, C. Y., Liao, J. T, and Lin, H. D., (1998) Performance of diaphragm wall constructed using top-down method. Journal of Geotechnical and Geoenvironmental Engineering, ASCE, Vol. 124, No. 9, pp. 798-808.

Ou, C. Y., Shiau, B. Y. and Wang, I. W., (2000) Three-dimensional deformation behavior of the Taipei National Enterprise Center (TNEC) excavation case history. Canadian Geotechnical Journal, Vol. 37, pp. 438-448.

Roscoe, K. H. and Burland, J.B., (1968) On the generalized stress–strain behaviour of 'wet' clay. In: Heyman, J., Leckie, F.A. (Eds.), Engineering Plasticity. Cambridge University Press, pp. 535-609.

Whittle, A. J., Hashash, Y. M. A. and Whitman, R. V., (1993) Analysis of deep excavation in Boston. Journal of Geotechnical Engineering, ASCE, Vol. 119, No. 1, pp. 69-90.

Zdravkovic, L., Potts, D. M. and St. John, H. D., (2005) Modelling of a 3D excavation in finite element analysis. Géotechnique, Vol. 55, No. 7, pp. 497-513.